NASA Technical Memorandum 106789

Modeling of Stress/Strain Behavior of Fiber-Reinforced Ceramic Matrix Composites Including Stress Redistribution

Subodh K. Mital
The University of Toledo
Toledo, Ohio

Pappu L.N. Murthy and Christos C. Chamis
Lewis Research Center
Cleveland, Ohio

December 1994

National Aeronautics and Space Administration

MODELING OF STRESS/STRAIN BEHAVIOR OF FIBER-REINFORCED CERAMIC MATRIX COMPOSITES INCLUDING STRESS REDISTRIBUTION

Subodh K. Mital
The University of Toledo
Toledo, Ohio 43606

Pappu L.N. Murthy and Christos C. Chamis
National Aeronautics and Space Administration
Lewis Research Center
Cleveland, Ohio 44135

ABSTRACT

A computational simulation procedure is presented for nonlinear analyses which incorporates microstress redistribution due to progressive fracture in ceramic matrix composites. This procedure facilitates an accurate simulation of the stress-strain behavior of ceramic matrix composites up to failure. The nonlinearity in the material behavior is accounted for at the constituent (fiber/matrix/interphase) level. This computational procedure is a part of recent upgrades to CEMCAN (CEramic Matrix Composite ANalyzer) computer code. The fiber substructuring technique in CEMCAN is used to monitor the damage initiation and progression as the load increases. The room-temperature tensile stress-strain curves for SiC fiber reinforced reaction-bonded silicon nitride (RBSN) matrix unidirectional and angle-ply laminates are simulated and compared with experimentally observed stress-strain behavior. Comparison between the predicted stress/strain behavior and experimental stress/strain curves is good. Collectively the results demonstrate that CEMCAN computer code provides the user with an effective computational tool to simulate the behavior of ceramic matrix composites.

INTRODUCTION

Ceramic matrix composites (CMC's) are currently a subject of a great deal of research interest due to the requirement for new high temperature materials for use in high speed engine structural components and other applications. Continuous-fiber reinforced ceramic matrix composites offer promise in this area and hence considerable effort is being devoted for their development. They offer several advantages such as high specific stiffness and strength, higher toughness and nonbrittle failure as compared to monolithic ceramics, environmental stability and wear resistance for both room and elevated temperature applications.

There are several differences between ceramic matrix and, say, polymer matrix composites. In polymer matrix composites, the fibers provide stiffness, while the polymer matrix serves primarily as a binder and generally has a very low modulus. The ratio of Young's modulus of the fibers and matrix is typically of the order of $O(10^2)$ in these composites. In addition, to achieve high stiffness it is usually desirable to have a strong interfacial bond between the fiber and matrix materials. On the other hand, a major role of fibers in ceramic matrix composites in addition to providing higher stiffness, is to provide mechanisms to enhance toughness as the matrix material is quite brittle and fails at relatively low strain levels. The ratio of the Young's modulus of the fibers and matrix materials in ceramic matrix composites is typically of the order of $O(10^0)$. It is desirable to have a weak interfacial bonding between the fibers and matrix in CMC's to enable such toughening mechanisms as fiber debonding, fiber bridging, fiber pullout, crack deflection etc. in order to eliminate catastrophic failures and to provide some ductility. Therefore, in spite of some similarities with polymer matrix, the analysis of ceramic matrix composites requires an entirely different approach. CEramic Matrix Composite ANalyzer (CEMCAN) has been under continued development under the sponsorship of HITEMP (HIgh Temperature Engine Materials Program) at NASA Lewis Research Center in Cleveland, Ohio to achieve this goal. CEMCAN is based upon composite micro-, meso- and macromechanics and has been developed specifically to simulate aspects unique to CMC's. It incorporates a novel and unique fiber substructuring technique that has many advantages including a more accurate micromechanical representation of interfacial conditions, both around the fiber and through-the-thickness of the laminate, and provides a greater detail in stress distribution within a ply at a very high computational efficiency as compared to numerical analysis techniques used for micromechanical analyses. Recently, a nonlinear analysis capability which includes the local stress redistribution due to progressive fracture has been added to the CEMCAN computer code.

The objectives of this paper are to describe the new features of the CEMCAN computer code and demonstrate its capabilities by simulating room-temperature tensile stress-strain curves up to failure of both unidirectional and angle-ply laminates of SiC/RBSN composites at room temperature.

CEMCAN COMPUTER CODE

In-house research at NASA Lewis Research Center in Cleveland, Ohio over the past two decades has resulted in several computer codes for composite micromechanics, mesomechanics and macromechanics. The primary intention of this research is to develop composite mechanics theories and analysis methods that range in scale from micromechanics to global structural analysis in one integrated code. The micromechanics theories are represented by simplified equations. Among the codes that have resulted from this effort are ICAN (Integrated Composite Analyzer) (ref. 1) and METCAN (Metal Matrix Composite Analyzer) (ref. 2). The ICAN computer code which is developed for the analysis of polymer matrix composites uses a representative volume element (RVE) that consists of fiber and matrix. A perfect bonding condition is assumed between the two constituents. The unit cell or RVE for METCAN, which is developed for the analysis of metal matrix composites, consists of fiber, matrix and an optional third phase called interphase. The interphase is treated as a distinct region with distinct mechanical and thermal properties which can be different than those of fiber or matrix. Thus, the interphase can represent a reaction zone formed due to the chemical reaction between fiber and matrix or a fiber coating or a layer provided intentionally to prevent such a reaction. This approach has been taken one step further for the analysis of ceramic matrix composites. Although, the same square fiber array pattern is used as in the previous codes, the fiber in the unit cell or RVE is divided into several slices. The composite micromechanics equations are derived for the slices rather the RVE. The equivalent properties of the RVE are derived by the application of classical laminate theory. The advantages of fiber substructuring technique and related micromechanics equations were described in reference 3. These equations have been programmed into the computer code CEMCAN. The flow-chart of the CEMCAN computer code is shown in figure 1. The left side of the chart shows the various steps involved in the synthesis of the properties from slice to laminate level, while the right side of the chart shows the various steps involved in the decomposition of the response from laminate to ply, to slice and then to microstresses. Composite micromechanics equations are used to determine the equivalent elastic properties of a composite material in terms of the elastic properties of its constituent materials. The properties of interest are composite moduli, Poisson's ratios, thermal expansion coefficients, thermal conductivities, heat capacities etc. The ply/fiber substructuring is shown schematically in figure 2. This technique allows a more accurate micromechanical representation of the composite material and at the same time, provides a greater detail in local stress distribution within a ply.

Recently, a nonlinear analysis capability that incorporates local stress redistribution due to progressive fracture has been added to the CEMCAN computer code. The material nonlinearity is accounted for at the constituent (fiber/matrix/interphase) level. For example, the constituent material properties as a function of temperature during the fabrication/cool-down process can be easily accounted for while computing the residual stresses. This capability allows for the inclusion of residual stresses that arise due to the temperature difference between the processing and the use temperatures and the mismatch in the coefficients of thermal expansion of the fiber and matrix materials prior to the application of any loading and simulates the stress/strain state in the as-fabricated material. The other capability that has been added is microstress redistribution as the fracture initiates and propagates in a laminate. If a constituent fails in a slice, it unloads and its microstresses are redistributed to the unfailed regions. This capability is described in more detail in a later section.

MULTIFACTOR INTERACTION RELATIONSHIP

Research over the last two decades at NASA Lewis Research Center to simulate the behavior of composite materials has culminated in a unified law to describe the material degradation behavior. This unified law, referred to as the multifactor interaction relationship (MFIR), takes into account the degradation effect on constituent material behavior due to environmental, fabrication and load effects. A generic form of the above mentioned MFIR is given by:

$$\frac{P}{P_0} = \prod_{i=1}^{n} \left[\frac{V_f - V}{V_f - V_0} \right]_i^a \tag{1}$$

where

P current property
P_0 reference property
V current value of the primitive variable representing load/environmental effect

superscript

a exponent for a given effect

subscript

f final value of the variable
0 reference value of the variable (e.g. for temperature effect, V_0 can be room-temperature)

Any number of effects and their interaction on a given material property can be described. The exponents are determined from available experimental data or sometimes estimated from anticipated material behavior based on an educated guess. The nonlinearity in the overall composite behavior also arises due to microfracture and subsequent microstress redistribution as the fracture initiates and propagates. In the present work, the constituent properties namely the modulus and coefficient of thermal expansion are considered a function of temperature only. Hence, for the modulus for example, the above equation (1) reduces to:

$$\frac{E}{E_0} = \left[\frac{T_f - T}{T_f - T_0}\right]^a \tag{2}$$

where

E is the modulus at temperature T
E_0 is the reference modulus at temp T_0 (usually modulus at room-temperature)
T_f is the final temperature where the modulus is zero

MICROSTRESS REDISTRIBUTION DUE TO PROGRESSIVE FRACTURE

A unique capability to carry-out a progressive fracture analysis with microstress redistribution resulting from progressive fracture has been added to the CEMCAN computer code. Once the microstresses are computed in all the constituents of a slice, they are compared with the current corresponding strengths. The maximum stress criterion for failure is used in the current analysis. The constituents are assumed to be void or flaw free. Although, for brittle materials, the strength values may depend upon the size and distribution of flaws, this failure criterion does not account for such effects. A statistical/probabilistic analysis should be carried out to accurately account for the effect of flaw size and distribution on the strength of a constituent. If a constituent stress has exceeded the corresponding strength value, then the constituent is assumed to have failed and the corresponding modulus of that constituent is reduced to an almost negligible value. A slice is assumed to have failed in the longitudinal direction if there is a fiber failure in that slice in the longitudinal direction. A matrix failure in the transverse or shear direction means the slice has failed in the transverse or shear direction respectively. Once a slice fails, all the microstresses that are carried by that slice up to that load step are redistributed in the slices that have not failed. The load redistribution due to progressive fracture is shown schematically in figure 3. The load that was carried by the failed slice is then added appropriately to the laminate load (as shown in fig. 3), and a laminate analysis is carried out again. This process is continued for a given load step until an equilibrium (convergence) state is reached between the applied load and a damage state. Presently, the convergence is checked for laminate mid-plane strains, ply and slice strains. Once all the strains are within 5 percent of the previous iteration,

convergence is assumed to have been reached. This mechanism is mainly responsible for the overall nonlinear behavior in the laminate tensile stress-strain curves at room-temperature.

RESULTS/DISCUSSION

The composite system used here is SiC/RBSN (silicon carbide SCS-6 fibers in a reaction bonded silicon nitride Si_3N_4 matrix) as mentioned before. The fiber and matrix mechanical and thermal properties, shown here in table I, have been provided in reference 4. This composite system is known to have a very compliant and weak interphase. The thickness of the interphase, a combination of outer carbon layer of the fiber and any reaction zone, is estimated to be approximately 3 percent of the fiber diameter ($0.03 \times 142 = 4.3$ μm). However, the thermal and mechanical properties of the interphase are not known. The nominal fiber volume ratio for this composite was estimated in the range of 0.3 to 0.34 in reference 5. Since it is well known that the interphase properties have very little effect on the longitudinal modulus of a unidirectional composite (ref. 6), the nominal fiber volume ratio (fvr) is calibrated to be 0.36 by comparing the measured and predicted values of longitudinal modulus for a unidirectional composite (fiber and matrix modulus are known). It should be mentioned here that in the simulation process, the formation of the interphase degrades the fiber. Hence, the effective fiber diameter is reduced and so is the fiber volume ratio but the matrix volume ratio remains unchanged. For example, in the present analysis, the gross fiber volume ratio is 0.36, fiber diameter is 142 μm, interphase thickness is 3 percent of the fiber diameter, then effectively fiber volume ratio reduces to 0.318, interphase volume ratio is 0.042 and matrix volume ratio remains unchanged at 0.64 (1 to 0.36). Once the nominal fvr is known, the interphase modulus is calibrated by comparing the measured and predicted values of transverse modulus for a unidirectional composite since the transverse composite modulus is quite sensitive to interfacial conditions. Alternatively, the measured value of in-plane shear modulus for a unidirectional composite can also be used to calibrate the interphase shear modulus. Once calibrated, these values were used to predict some mechanical properties for two laminates $[0_2/90_2]_s$ and $[\pm 45_2]_s$ and these predictions were compared with experimentally measured values. Results are shown in table II. The comparison is excellent, except for ν_{12} for $[\pm 45_2]_s$ laminate and all the predictions are within the scatter of the measured values. This calibration process is explained in little more detail in reference 4. A linear laminate analysis was also performed on a unidirectional composite and microstresses were computed for different types of applied loading. Although the results are not shown here, those resulting microstresses were compared with the predictions of a detailed three-dimensional finite element analyses and the results were in very good agreement.

In the present work, the tensile stress-strain behavior up to failure for unidirectional on- and off-axis specimens and two angle-ply laminates is predicted and compared with experimental stress-strain curves at room temperature. The fabrication of these composites is explained in Ref. 5. These composites are processed (i.e., nitridation is performed) between 1200 to 1400 °C. However, after performing several analyses, the stress free temperature in the present simulations is assumed to be 900 °C in order to obtain the observed failure modes in these composites. This suggests that at higher temperatures (900 to 1200 °C) some metallurgical mechanism is operative that prevents stress build-up above the assumed stress-free temperature (900 °C). Such observations have been made before with regards to other ceramic matrix composites (ref. 7). In the present simulations, the composites are cooled down to room-temperature (20 from 900 °C) prior to application of any loading. It is also mentioned that the maximum use temperature of these composites will be around 1200 °C and there is very little degradation (maximum 10 percent, ref. 8) in constituent modulus etc. even at the maximum use temperature compared to the reference property at room temperature. To take that into account, the exponent for the temperature dependence of the properties (modulus and coefficient of thermal expansion) is taken as 0.25 for the fiber and 0.1 for the matrix, final temperature (T_f, equation (2)) is taken as 2500 °C for the fiber and 2200 °C for the matrix material. These assumed values would correspond to the observed degradation in the constituent material properties, namely modulus and thermal expansion coefficient for the range of the use temperature for these material.

Room-temperature stress-strain curves for both $[0]_8$ and $[90]_8$ composites are shown in figure 4. Based on the observed tensile strengths of $[0]_8$ and $[90]_8$ composites, matrix in-situ tensile strength was calibrated as 100 MPa (14.5 ksi) and average fiber bundle strength as 2 GPa (285 ksi) by comparing the knee in the stress-strain curve of $[0]_8$ composite i.e., the deviation in the linear behavior and the fiber strength is calibrated by comparing the final failure stress of the same composite. These values agree well with the fiber and matrix tensile strengths reported in reference 5. Once calibrated, the same strengths values were used in subsequent simulations. For the $[0]_8$ composite, stress-strain curve is linear initially as both fiber and matrix are intact. Upon further loading, the matrix starts cracking until saturation is reached. Consequently, all the load is carried by the fibers only, which is represented by the second linear region of the stress-strain curve. Final fracture occurs when the fibers fail in all the plies. Such an observation agrees very well with the optical

observations made of specimens loaded to different stress levels (ref. 5). The $[90]_8$ composite shows linear behavior until failure. It failed with the failure of matrix in the transverse tension, at a relatively low stress level of 45 MPa.

In contrast, the off-axis laminates $[10]_8$ and $[45]_8$ stress-strain behavior is largely linear up to failure as shown in figure 5. Such a behavior is characteristic of a brittle failure. The final fracture in these laminates is controlled by a combination of matrix/interphase normal and shear failure modes. Optical micrographs shown in reference 5 are in agreement with such failure modes. Room-temperature stress-strain curve to failure for a $[\pm 45]_s$ laminate is shown in figure 6. The shear strength of the matrix is estimated to be half of the matrix tensile strength to match the ultimate stress of $[\pm 45_2]_s$ laminate. This laminate also fails in a combination of shear and normal failure modes and shows the characteristics of a graceful failure. Once again, the predicted strength of this laminate matches well with the experimentally measured value, and the optical micrographs in reference 5 confirm the above mentioned failure modes. The unloading part of the stress-strain curve for a $[\pm 45_2]_s$ laminate is not predicted.

The room-temperature stress-strain curve to failure for a cross-ply laminate $[0_2/90_2]_s$ is shown in figure 7. Up to a stress level of 150 to 200 MPa, the curve is linear and shows no damage. The initial modulus agrees well with the experimental measurement. Damage initiates, first in the form of fiber matrix debonding in the 90° plies and subsequently as matrix cracking in the 0° plies. In the second linear region of the stress-strain curve, the 90° plies are fully cracked and do not contribute to the stiffness in the loading direction and the matrix is fully saturated with cracks in the 0° plies and does not contribute to the stiffness in the loading direction either. All the load at this point is carried by fibers only in the 0° plies. However, the slope of the second linear portion of the stress-strain curve is higher than that of the observed stress-strain behavior. The experimental curve suggests that all the fibers in the 0° plies are not contributing to the stiffness. One possible explanation is that there is probable damage due to processing in the fibers of 0° plies. All the 0° fibers are not contributing to the stiffness in the second linear portion of the stress-strain curve. Comparing the slope of the second linear portion of the stress-strain curve, it would appear that the fiber volume ratio of 0° plies is approximately half, i.e., experimental stress-strain curve slope of the second linear portion is approximately half of the slope of the predicted curve. The fiber lay-out for this laminate is shown in figure 8. It is possible that during the processing/composite fabrication, the application of high pressure at relatively high temperature, will result in impingement of 90° fibers on to the inner 0° fibers, resulting in some damage to the inner 0° fibers. If both the inner fibers were damaged, that will be two fibers out of four in the loading direction, and would corroborate with the earlier observation that only half of the fibers in loading direction seem to be effective. Damage to the fibers due to processing could result in a shift in the mean strength of fibers (fig. 8) causing premature fiber failure. Although the predicted stress-strain curve accounts for the residual stresses resulting from the processing of the composite, it assumes no damage in the 0° fibers and thus results in a much stiffer behavior and a higher strength value. In fact, the experimentally measured strength value for this laminate (290 MPa) is bound by the predicted strength with no damage in the fibers, 390 MPa (upper bound) and with both inner 0° fibers damaged, 195 MPa (lower bound).

SUMMARY/CONCLUSIONS

Recent upgrades to the CEMCAN computer code including nonlinear analysis capability with microstress redistribution due to progressive fracture are described. Collectively, the results presented show that CEMCAN provides sufficient flexibility to the user to study various aspects in the deformation/fracture behavior of ceramic matrix composites. Based on the results presented and discussed, it can be concluded that:

1. Unidirectional $[0]_8$ composite loaded along longitudinal direction displays linear stress-strain behavior up to first matrix cracking stress. Beyond this point, matrix is ineffective and all the load is carried by the fibers until fracture.
2. Off-axis and angle-ply laminates tensile strength is governed by a combination of matrix/shear failure.
3. There is probable fiber damage/breakage due to processing in the cross-ply $[0_2/90_2]_s$ laminate.
4. CEMCAN computer code provides the user with a "virtual test laboratory," in that the new candidate materials, different laminate configurations or service environments can be evaluated in a fraction of time and cost, with only a minimum number of tests needed for the calibration of certain material properties for a given material system.

REFERENCES

1. Murthy, P.L.N.; Ginty, C.A.; and Sanfeliz, J.G.: Second Generation Integrated Composite Analyzer (ICAN) Computer Code. NASA TP–3290, 1993.

2. Lee, H.-J.; Gotsis, P.K.; Murthy, P.L.N.; and Hopkins, D.A.: Metal Matrix Composite Analyzer (METCAN) User's Manual - Version 4.0 NASA TM–105244, 1991.
3. Murthy, P.L.N.; and Chamis, C.C.: Towards the Development of Micromechanics Equations for Ceramic Matrix Composites via Fiber Substructuring. NASA TM–105246, 1992.
4. Mital, S.K.; Murthy, P.L.N.; and Chamis, C.C.: Ceramic Matrix Composites Properties/Microstresses With Complete and Partial Interphase Bond. NASA TM–106136, 1993.
5. Bhatt, R.T.; and Phillips, R.E.: Laminate Behavior for SiC Fiber-Reinforced Reaction-Bonded Silicon Nitride Matrix Composites. NASA TM–101350, 1988.
6. Mital, S.K.; Murthy, P.L.N.; and Chamis, C.C.: Ceramic Matrix Composites: Effect of Local Damage on Composite Response. Proc. 6th Annual HITEMP Review, NASA CP–19117, 1993.
7. Rousseau, C.Q.; Davidson, D.L.; and Campbell, J.B.: The Micromechanics of Ambient Temperature Cyclic Fatigue Loading in a Composite of CAS Glass Ceramic Reinforced with Nicalon Fibers. Journal of Composites Technology & Research, Vol. 16, No. 2, April 1994, pp. 115–126.
8. Bhatt, R.T., Private communication, NASA Lewis Research Center, Cleveland, Ohio, 1994.

TABLE I.—CONSTITUENT PROPERTIES OF SIC/RBSN AND PROPERTIES OF $[0]_8$ COMPOSITE CONSTITUENT PROPERTIES

Property	SiC (SCS-6) fiber		RBSN matrix		Interphase	
Modulus, GPa (Msi)	390	(56.6)	110	(15.95)	3.5 (calculated)	(0.5)
Poisson's ratio	0.17		0.22		0.22	
Shear modulus, GPa (Msi)	117	(17)	45	(6.5)	1.4	(0.2)
Coefficient of thermal expansion, 10^{-6}/°C (10^{-6}/°F)	4.1	(2.3)	2.2	(1.2)	2.0	(1.1)
Thermal conductivity, W/m-K (Btu/ft-h °F)	22	(12.7)	5	(2.9)	2.0	(1.2)

UNIDIRECTIONAL SIC/RBSN $[0]_8$ COMPOSITE FIBER VOLUME RATIO 0.36[a]

Property	Predicted		Measured[b]	
E_{11}, GPa (Msi)	189	(27.4)	193±7	(28±1)
E_{22}, GPa (Msi)	68.3	(9.9)	69±3	(10±0.4)
G_{12}, GPa (Msi)	27	(3.9)	31±3	(4.5±0.4)
ν_{12}	0.21		0.2	

[a]Note: The measured value of longitudinal modulus for a unidirectional composite, E_{11}, was used to compute fiber volume ratio (fvr), while the transverse modulus, E_{22}, was used to compute the interphase modulus.
[b]Reference 3.

TABLE II.—COMPARISON OF PREDICTED (CEMCAN) AND MEASURED ELASTIC PROPERTIES OF SIC/RBSN LAMINATES

Property	$[0_2/90_2]_s$ laminate		$[\pm 45_2]_s$ laminate	
	Predicted	Measured[a]	Predicted	Measured[a]
E_{11}, GPa (Msi)	129 (18.7)	124±6 (18±0.9)	78.6 (11.4)	78±3 (11.3±0.4)
E_{22}, GPa (Msi)	129 (18.7)	124±6 (18±0.9)	78.6 (11.4)	78±3 (11.3±0.4)
G_{12}, GPa (Msi)	27 (3.9)	31±2 (4.5±0.3)	58 (8.4)	----------
ν_{12}	0.112	0.12	0.46	0.36

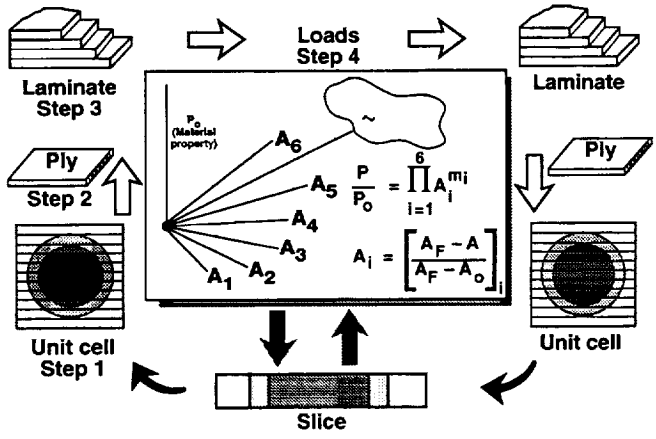

Figure 1.—Integrated analysis approach embedded in CEMCAN computer code.

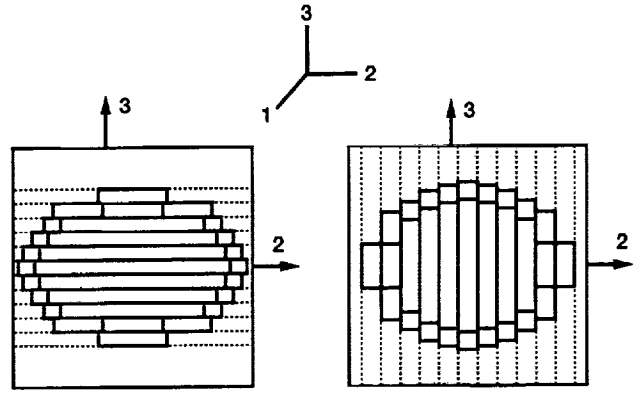

(Note: 1-1 is along the fiber direction)

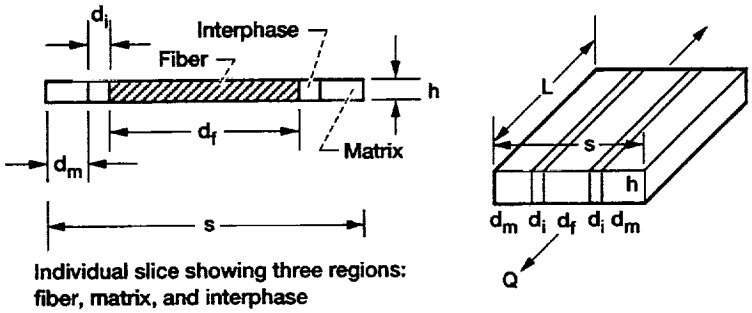

Individual slice showing three regions: fiber, matrix, and interphase

Figure 2.—Ply/fiber substructuring concepts for ceramic matrix composites micromechanics.

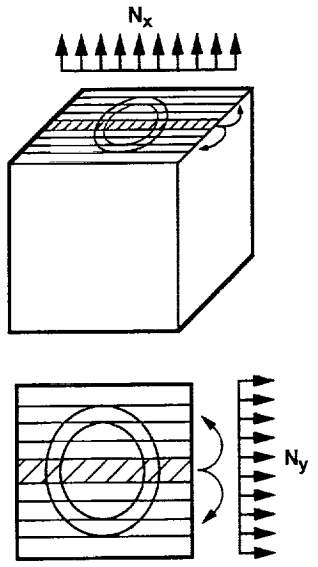

- Failure based on maximum stress criterion
- Fiber failure governs the failure of slice in the longitudinal direction
- $N_x' = N_x + s_{slice\ 11} \times$ (slice thickness)
- Matrix/interphase failure governs the slice failure in transverse (shear) loading
- $N_y' = N_y + s_{slice\ 22} \times$ slice thickness)

Figure 3.—Local stress redistribution due to progressive fracture.

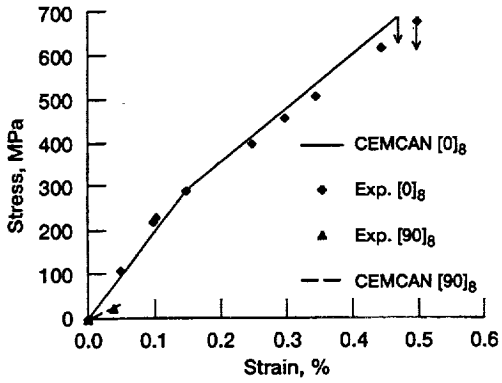

Figure 4.—Room-temperature stress-strain curves to failure of $[0]_8$ and $[90]_8$ SiC/RBSN composite.

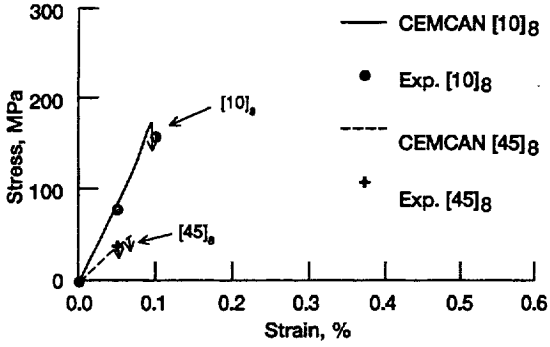

Figure 5.—Room-temperature stress-strain curves to failure of $[10]_8$ and $[45]_8$ laminates of SiC/RBSN.

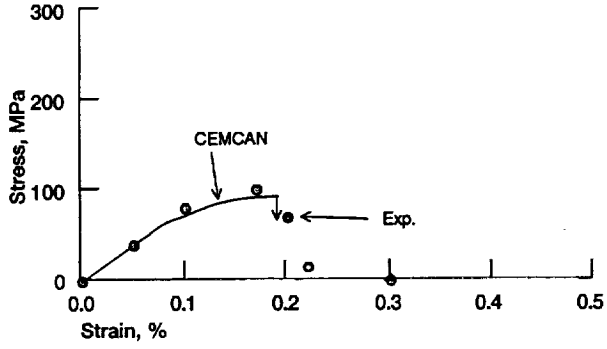

Figure 6.—Room-temperature stress-strain curves to failure of $[+45/-45]_S$ SiC/RBSN laminate.

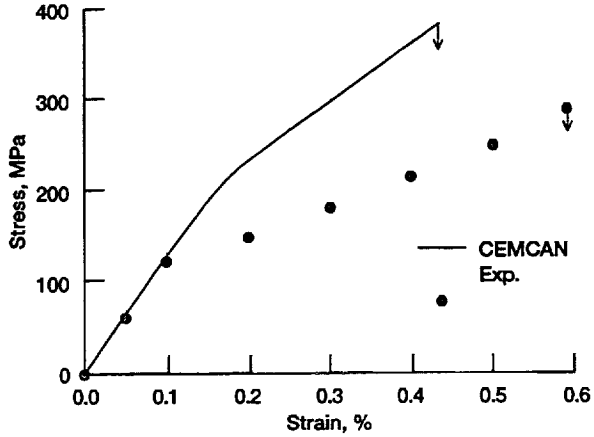

Figure 7.—Room-temperature tensile stress-strain curve to failure of $[0_2/90_2]_S$ cross-ply laminate of SiC/RBSN.

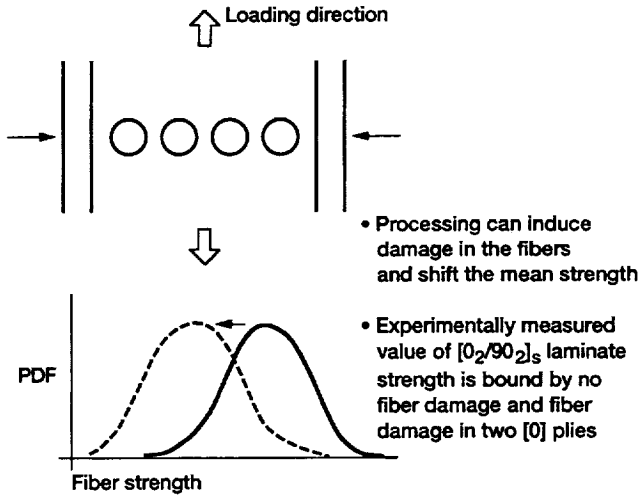

Figure 8.—Fiber layout for $[0_2/90_2]_S$ laminate.

REPORT DOCUMENTATION PAGE

Form Approved
OMB No. 0704-0188

1. AGENCY USE ONLY (*Leave blank*)	2. REPORT DATE	3. REPORT TYPE AND DATES COVERED
	December 1994	Technical Memorandum

4. TITLE AND SUBTITLE

Modeling of Stress/Strain Behavior of Fiber-Reinforced Ceramic Matrix Composites Including Stress Redistribution

5. FUNDING NUMBERS

WU-505-63-12

6. AUTHOR(S)

Subodh K. Mital, Pappu L.N. Murthy, and Christos C. Chamis

7. PERFORMING ORGANIZATION NAME(S) AND ADDRESS(ES)

National Aeronautics and Space Administration
Lewis Research Center
Cleveland, Ohio 44135-3191

8. PERFORMING ORGANIZATION REPORT NUMBER

E-9249

9. SPONSORING/MONITORING AGENCY NAME(S) AND ADDRESS(ES)

National Aeronautics and Space Administration
Washington, D.C. 20546-0001

10. SPONSORING/MONITORING AGENCY REPORT NUMBER

NASA TM-106789

11. SUPPLEMENTARY NOTES

Subodh K. Mital, The University of Toledo, Toledo, Ohio 43606; Pappu L.N. Murthy and Christos C. Chamis, NASA Lewis Research Center. Responsible person, Pappu L.N. Murthy, organization code 5210, (216) 433-3332.

12a. DISTRIBUTION/AVAILABILITY STATEMENT

Unclassified - Unlimited
Subject Category 24

12b. DISTRIBUTION CODE

13. ABSTRACT (*Maximum 200 words*)

A computational simulation procedure is presented for non-linear analyses which incorporates micro-stress redistribution due to progressive fracture in ceramic matrix composites. This procedure facilitates an accurate simulation of the stress-strain behavior of ceramic matrix composites up to failure. The non-linearity in the material behavior is accounted for at the constituent (fiber/matrix/interphase) level. This computational procedure is a part of recent upgrades to CEMCAN (CEramic Matrix Composite ANalyzer) computer code. The fiber substructuring technique in CEMCAN is used to monitor the damage initiation and progression as the load increases. The room-temperature tensile stress-strain curves for SiC fiber reinforced reaction-bonded silicon nitride (RBSN) matrix unidirectional and angle-ply laminates are simulated and compared with experimentally observed stress-strain behavior. Comparison between the predicted stress/strain behavior and experimental stress/strain curves is good. Collectively the results demonstrate that CEMCAN computer code provides the user with an effective computational tool to simulate the behavior of ceramic matrix composites.

14. SUBJECT TERMS

Ceramic matrix composites; Stress; Strain; Interphase; Interface; Damage; Fracture; Fiber; Silicon carbide fiber; Silicon nitride matrix; Simulation

15. NUMBER OF PAGES

11

16. PRICE CODE

A03

17. SECURITY CLASSIFICATION OF REPORT	18. SECURITY CLASSIFICATION OF THIS PAGE	19. SECURITY CLASSIFICATION OF ABSTRACT	20. LIMITATION OF ABSTRACT
Unclassified	Unclassified	Unclassified	

National Aeronautics and
Space Administration

Lewis Research Center
21000 Brookpark Rd.
Cleveland, OH 44135-3191